Thermal Science and Engineering (2023) Volume 6 Issue 2
doi: 10.24294/tse.v6i2.4424

ORIGINAL RESEARCH ARTICLE

Impact of separator thickness on relationship between temperature distribution and mass & current density distribution in single HT-PEMFC

Akira Nishimura[1,*], Daiki Mishima[1], Syogo Ito[1], Tsubasa Konbu[1], Eric Hu[2]

[1] *Division of Mechanical Engineering, Mie University, Tsu 514-8507, Japan*

[2] *School of Mechanical Engineering, the University of Adelaide, Adelaide 5005, Australia*

*** Corresponding author:** Akira Nishimura, nisimura@mach.mie-u.ac.jp

ABSTRACT

Considering the application of the polymer electrolyte membrane fuel cell (PEMFC), the separator thickness plays a significant role in determining the weight, volume, and costs of the PEMFC. In addition, thermal management, i.e., temperature distribution is also important for the PEMFC system to obtain higher performance. However, there were few reports investigating the relation between the temperature profile and the power generation characteristics e.g., the current density distribution of PEMFC operated at higher temperatures (HT-PEMFC). This paper aims to study the impact of separator thickness on the temperature profile and the current density profile of HT-PEMFC. The impact of separator thickness on the gases i.e., H_2, O_2 profile of HT-PEMFC numerically was also studied using CFD software COMSOL Multiphysics in the paper. In the study, the operating temperature and the relative humidity (RH) of the supply gas were varied with the separator thickness of 2.0 mm, 1.5 mm, and 1.0 mm, respectively. The study revealed that the optimum thickness was 2.0 mm to realize higher power generation of HT-PEMFC. The heat capacity of the separator thickness of 2.0 mm was the biggest among the separators investigated in this study, resulting in the dry-up of PEM and catalyst layer was lower compared to the thinner separator thickness. It also clarified the effects of separator thickness of profile gases, e.g., O_2, H_2O, and current density profile became larger under the higher temperature and the lower RH conditions.

Keywords: HT-PEMFC; numerical simulation; separator thickness; coupling phenomena

ARTICLE INFO

Received: 26 July 2023
Accepted: 22 August 2023
Available online: 1 September 2023

1. Introduction

The Japanese New Energy and Industry Technology Development Organization (NEDO), which is a Japanese government agency, has announced that polymer electrolyte membrane fuel cells (PEMFC) should be worked at a higher temperature, such as 363 K and 373 K, for the application of stationary and vehicles, respectively, during the period from 2020 to 2025 in road map 2017[1]. On the other hand, PEMFC, which uses a Nafion membrane for a polymer electrolyte membrane (PEM), generally works below 353 K[2–4]. The merits of PEMFC operated at higher temperatures (HT-PEMFC) include (i) kinetic improvement of the catalyst; (ii) downscale effect of the cooling system for mobility applications thanks to the increase in temperature gap between the PEMFC stack and coolant; and (iii) enhancement of CO endurance, allowing the purity of H_2 production from hydrocarbons such as CH_4[5]. On the other hand, the following issues should be overcome: (i) degradation of PEM because of thermal expansion and shrinkage, (ii) electrode erosion, (iii) an uneven profile of gas flow, gas pressure, temperature, voltage, and current density in

PEMFC[6]. In addition, the uneven profiles of H_2, O_2, H_2O, temperature, and current density would undermine the power generation characteristics as well as the operation life of PEMFC when operated at higher temperatures than usual. However, as to the existing PEMFC, the following problems are considered[7,8]; (1) low tolerance of cartalyst such as Pt to contaminants such as CO, (2) slow electrochemical kinetics, (3) difficulties in the water and thermal management. These problems can be solved under higher operation temperature conditions (HT-PEMFC).

The effect of the thickness of PEM and gas diffusion layer (GDL) as well as a microporous layer (MPL) on the coupling phenomena of HT-PEMFC worked at 363 K and 373 K had been studied experimentally and numerically[9–11] by authors. Moreover, the effect of separator thickness on H_2, O_2, H_2O, and current density distributions has been investigated numerically[12] and on the temperature profile on the separator's back surface experimentally[13]. According to recent works except for the authors' studies[12,13], the impact of the interdigitated flow field of the separator on mass transport and electrochemical reactions in HT-PEMFC was investigated by the CFD software COMCOL multiphysics[14]. Compared to the performance of the interdigitated flow field with that of the parallel flow field, the increase in current density with air stoichiometry in the case of the integrated flow field was approximately three times as large as that in the case of the parallel flow field. On the other hand, the polarization curve in the case of an interdigitated flow field was almost the same as that in the case of a single-channel serpentine flow field. Though the relationship between O_2 distribution or pressure distribution and the power generation performance was discussed, that between the temperature distribution and the power generation performance was not investigated. The other numerical study using CFD software COMCOL Multiphysics reported that three different types of cathode-enhanced mass transfer flow fields, i.e., tapered, staggered-blocked, and blocked were designed and their performances compared[15]. As a result, the tapered flow field was the optimum design for HT-PEMFC due to its superior performance and lower flow resistance. Though the relationship between the power generation characteristics and O_2 profile or flow field distribution was discussed, that between the power generation characteristics and the temperature distribution was not studied. Regarding the general PEMFC operated below 353 K, the several flow fields of the separator such as a modified parallel flow field[16], a blocked flow field[17], a modified serpentine wave flow filed[18], a straight channel with baffled obstacles[19] and an ultrathin steel separator whose thickness was 0.1 mm[20] were investigated. Foam structure separators consisting of graphene or metal to improve mass diffusion were investigated and compared to the normal separator[21,22]. The porous structure of foam can improve convection and diffusion and reduce the contact resistance between the flow plate and carbon paper. Since the weight ratio of the separator to that of the total cell is approximately 80%[23], it is important to optimize the design of the separator. Especially, the separator thickness has a big impact on the weight, volume, and cost of the cell. In addition, thermal management is important to realize higher performance for the application usage of the PEMFC system[24]. However, there are few reports investigating the relation between the temperature profile and the power generation characteristics, e.g., the current density profile of HT-PEMFC. Therefore, we aim to reveal the impact of separator thickness on the relationship between the temperature distribution and the current density distribution of HT-PEMFC. We have investigated the impact of separator thickness on the relationship between the temperature profile and the current density profile of HT-PEMFC numerically using the CFD software COMSOL Multiphysics. The reason why this study selected COMSOL Multiphysics is as follows: fuel cells improve complex multi-physics coupling problems, including charge transfer, water transport, heat transfer, etc. In COMSOL, users could select or customize various partial differential equations and combine them to achieve direct coupled multi-physics field analysis easily. As described above, some numerical studies on HT-PEMFC were conducted by COMSOL multiphysics[14,15]. Given the characteristics of fuel cells and the advantages of COMSOL software, we chose this software for the simulation work in this paper. The relation between the temperature profile and not only the current density profile but also the mass such as O_2 and H_2O profiles are also discussed. The separator thickness is changed by 2.0 mm, 1.5 mm, and 1.0 mm. The separator thickness of 2.0 mm consists of the saddle

thickness = 1.0 mm and the channel height = 1.0 mm. The separator thickness of 1.5 mm consists of the saddle thickness = 0.5 mm and the channel height = 1.0 mm. The separator thickness of 1.0 mm consists of the saddle thickness = 0.5 mm and the channel height = 0.5 mm. Regarding PEM and GDL, this study adopts Nafion NRE-211 and TGP-H-030, respectively. This selection follows the results obtained by the previous studies conducted by the authors, which optimized the thickness of PEM and GDL[12,13]. This study changes the operation temperature by 353 K, 363 K, and 373 K. This study investigates the characteristics at 353 K, 363 K, and 373 K. 353 K is selected as a case of LT-PEMFC for the comparison of the results under higher temperature conditions. The higher temperature conditions at 363 K and 373 K are selected following the target temperature for the application use of stationary and vehicles, respectively, during the period from 2020 to 2025 in the road map of NEDO. Compared to the general operation temperatures of HT-PEMFC of 413 K and 473 K, 363 K, and 373 K which are investigated in this study. However, issues such as low tolerance of catalysts such as Pt to CO and SO_2, difficulties in water and thermal management, and slow electrochemical kinetics can be improved over 373 K according to Zhang et al.[25]. Therefore, the 373 K investigated in this study has a point as a case study of HT-PEMFC. This study also examines changing the relative humidity (RH) of supply gases at the anode = 80%RH and cathode = 80%RH (A80%RH-C80%RH), anode = 80%RH and cathode = 40%RH (A80%RH-C40%RH), anode = 40%RH and cathode = 80%RH (A40%RH-C80%RH) and anode = 40%RH and cathode = 40%RH (A40%RH-C40%RH).

2. Numerical simulation procedure

Governing equation

The numerical simulation was conducted by multi-physics software, i.e., COMSOL Multiphysics, ver. 6.1. Fuel cells involve complex multi-physics coupling problems, including charge transfer, mass transfer, heat transfer, etc. In COMSOL, users could select or customize various partial differential equations and combine them to easily achieve directly coupled multi-physics field analysis. The COMSOL Multiphysics has a simulation function code consisting of the Brinkman formula, Maxwell-Stefan formula, Butler-Volmer formula, and heat transfer formula, considering the heat generated by overpotentials, thermal conduction through each component in the cell, thermal convection via the flow through the channel, as well as transferring from the exhaust gas to the ambient air. Some researchers previously carried out the numerical simulation using COMSOL Multiphysics for HT-PEMFC[4,14,15,25–28] and achieved good results for the temperature, gases, and current density distributions. In addition, the validation was conducted well. Thanks to the characteristics of fuel cells and the advantages of COMSOL, the present study adopted it for the numerical simulation of HT-PEMFC. The following governing equations are involved in COMSOL:

Firstly, the continuity equation treating the gas species in porous material in a single PEMFC, e.g., catalyst layer, MPL, GDL, and the gas channel, can be defined as follows:

$$\frac{\partial}{\partial t}\left(\varepsilon_p \rho\right) + \nabla \cdot \left(\rho \vec{u}\right) = Q_m \tag{1}$$

where ε_p is the porosity of porous material (-), ρ is the gas density (kg/m^3), $\vec{\mu}$ is the gas velocity vector (m/s), Q_m is the mass source term balancing this equation (kg/(m^3·s)), and t is the time (s).

The Brinkman equation, considering the relationship between gas pressure and gas flow velocity, which is solved in porous material in a single PEMFC, e.g., catalyst layer, MPL, GDL, and the gas channel, can be defined, as follows:

$$\frac{\rho}{\varepsilon_p}\left(\frac{\partial \vec{u}}{\partial t} + \left(\vec{u}\cdot\nabla\right)\frac{\vec{u}}{\varepsilon_p}\right) = -\nabla p + \nabla \cdot \left[\frac{1}{\varepsilon_p}\left\{\mu\left(\nabla \vec{u} + \left(\nabla \vec{u}\right)^T\right) - \frac{2}{3}\mu\left(\nabla \cdot \vec{u}\right)\vec{I}\right\}\right] - \left(\kappa^{-1}\mu + \frac{Q_m}{\varepsilon_p^2}\right)\vec{u} + \vec{F} \tag{2}$$

where p is the gas pressure (Pa), μ is the gas viscosity (Pa·s), $\vec{I}$ is the unit vector (-), κ is the permeability of

porous material (m^2), and $\vec{F}$ is the force vector ($kg/(m^2 \cdot s^2)$) such as gravity. The Maxwell-Stefan equation treating the mass transfer phenomena, i.e., the diffusion phenomenon, the ion transfer phenomenon, and the convection transfer phenomenon, can be defined as follows:

$$\vec{N_i} = -D_i \nabla C_i - z_i u_{m,i} F C_i \nabla \varphi_l + C_i \vec{u} = \vec{J_i} + C_i \vec{u} \tag{3}$$

$$\frac{\partial C_i}{\partial t} + \nabla \cdot \vec{N_i} = R_{i,tot} \tag{4}$$

where $\vec{N_i}$ indicates the vector molar flow rate on the interface between PEM and catalyst layer ($mol/(m^2 \cdot s)$), D_i indicates the diffusion constant of gas (m^2/s), C_i indicates the ion i concentration (mol/m^3), z_i indicates the ion valence (-), $u_{m,i}$ indicates the ion i mobility ($(s \cdot mol)/kg$), F indicates the faraday constant (C/mol), φ_l indicates the electrical potential of liquid material[28] (V), J_i indicates the molar flow rate of the convection transfer phenomenon ($mol/(m^2 \cdot s)$), and $R_{i,tot}$ indicates the species' reaction rate ($mol/(m^3 \cdot s)$).

The Butler-Volmer equation treats the electrochemical reaction phenomenon, as follows:

$$i = i_0 \left\{ \exp\left(\frac{\alpha_a F \eta}{RT} \right) - \exp\left(\frac{-\alpha_c F \eta}{RT} \right) \right\} \tag{5}$$

$$\eta = \varphi_s - \varphi_l - E_{eq} \tag{6}$$

where i is the current density (A/m^2), i_0 is the exchange current density (A/m^2), a_a is the charge transfer coefficient at anode side (-), η is the activation over-potential[29] (V), R is the gas constant ($J/(mol \cdot K)$), T is the operating temperature (K), a_c is the charge transfer constant at the cathode side (-), φ_s is the electrical potential of solid material[29] (V), E_{eq} is the equilibrium electric voltage[29] (V).

$$\rho C_p u \cdot \nabla T = \nabla \cdot (k \nabla T) + Q_{jh} + \sum_m a_v Q_m + q_0 \tag{7}$$

$$Q_{jh} = -\left(\vec{i_s} \cdot \nabla \varphi_s + \vec{i_l} \cdot \nabla \varphi_l \right) \tag{8}$$

$$Q_m = \left(\eta + T \frac{\delta E_{eq}}{\delta T} \right) i \tag{9}$$

$$q_0 = -h(T_{ext} - T) \tag{10}$$

where C_p indicates the constant pressure specific heat ($J/(kg \cdot K)$), k is the thermal conductivity ($W/(m \cdot K)$), a_c means the active area ratio (1/m), $\vec{i_s}$ means the electrode current density vector (A/m^2), $\vec{i_l}$ means the electrolyte current density vector (A/m^2), h indicates the heat transfer coefficient ($W/(m^2 \cdot K)$), T_{ext} indicates the external temperature (K).

The simulation model developed and used in this study was the same as the authors' previous study[12]. **Figure 1** illustrates the model for the separator thickness of 2.0 mm, 1.5 mm, and 1.0 mm. The structures of these models follow the commercial cell used in the experiments carried out by Nishimura et al.[11,13]. The separator has a serpentine flow channel consisting of five gas channels having a gas channel width of 1.0 mm and a gas channel width of 1.0 mm. This cell has five gas channels following the structure of the commercial cell[9,13]. This separator has the serpentine flow-field as shown in **Figure 2**. **Table 1** shows the geometrical parameters used for the model proposed in this study. **Tables 2** and **3** show physical parameters and operation conditions, respectively. We change the initial operation temperature of a cell (T_{ini}) by 353 K, 363 K, and 373 K. This study adopts 353 K to compare the characteristics obtained under usual temperature conditions with those at higher temperature conditions. We also change the RHs of supply gases i.e., A80%RH-C80%RH, A80%RH-C40%RH, A40%RH-C80%RH, and A40%RH-C40%RH. We examine the flow rate of supply gas in the case of the stoichiometric ratio (s.r.) of 1.5, where the volume flow rate of supply gas at the anode side and the cathode side is equal to 0.210 NL/min and 0.105 NL/min, respectively. The s.r. of 1.0 indicating the flow rate of supply gas can be expressed by Equation (11).

$$C_{H2} = \frac{I}{Z_{H2} F} \tag{11}$$

where C_{H2} is the molar flow rate of H_2 which is consumed in the electrochemical reaction (mol/s), I is the loaded current (A) and z_{H2} is the electrons moles which are exchanged in the reaction (=2) (-), C_{H2} is the molar flow rate for s.r. = 1.0. The C_{O2} is the molar flow rate of O_2 which is consumed in the electrochemical reaction (mol/s). The C_{O2} is half of C_{H2} (refer to Equation (12)).

$$H_2 + 1/2\ O_2 = H_2O \quad (12)$$

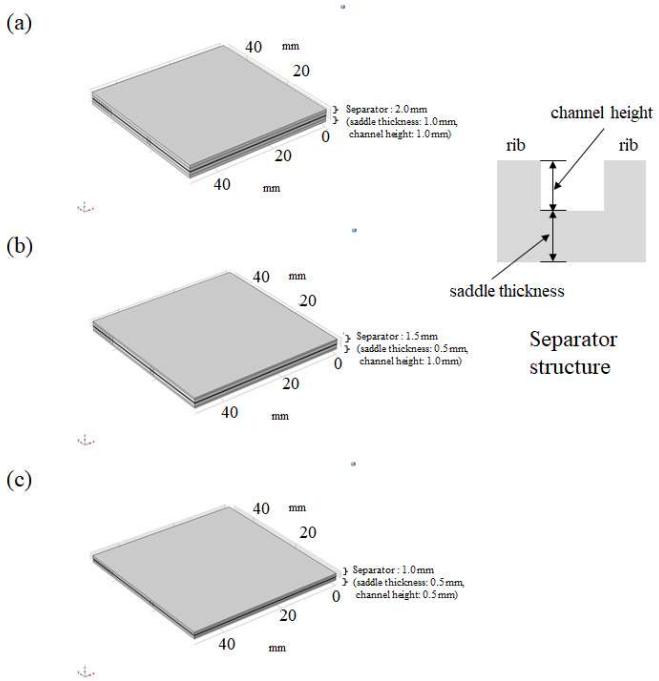

Figure 1. 3D model simulated for single HT-PEMFC (**(a)**: separator thickness of 2.0 mm, **(b)**: separator thickness of 1.5 mm, **(c)**: separator thickness of 1.0 mm).

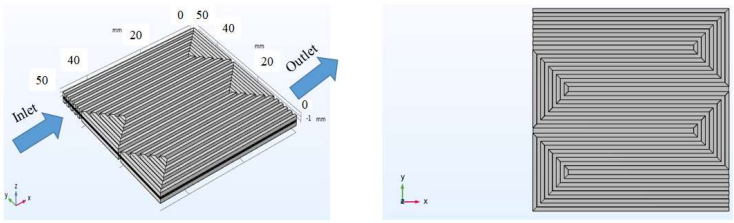

Figure 2. The 3D model simulated for single HT-PEMFC which shows the serpentine flow filed structure.

Table 1. Geometric parameters for components of model simulating single HT-PEMFC[10,14,30–33].

Components of single-cell	Each size[mm]	Specification
PEM	Width: 50.0, length: 50.0, depth: 0.025	Nafion NRE-212 (Manufactured by Du Pont Corp.)
Catalyst layer	Width: 50.0, length: 50.0, depth: 0.01	Pt/C (Weight percentage of Pt: 20)
MPL	Width: 50.0, length: 50.0, depth: 0.003	PTFE + carbon black
GDL	Width: 50.0, length: 50.0, depth: 0.11	TGP-H-030 (Produced by Toray Corp.)
Separator	Width: 75.4, length: 75.4, depth: 2.0 (saddle thickness: 1.0, channel height: 1.0), 1.5 (saddle thickness: 0.5, channel height: 1.0), 1.0 (saddle thickness: 0.5, channel height: 0.5); Width: 50.0, Length: 50.0 (as to gas supply area)	Carbon graphite, serpentine

Table 2. Physical parameters for gases, components of cells as well as electrochemical reactions.

Physical parameters	Values
Gas density (H_2) [kg/m^3]	7.10×10^{-2} (@ 353 K), 6.89×10^{-2} (@ 363 K), 6.69×10^{-2} (@ 373 K)[30]
Gas density (O_2) [kg/m^3]	1.11 (@ 353 K), 1.08 (@ 363 K), 1.05 (@ 373 K)[30]
Gas density (H_2O) [kg/m^3]	2.95×10^{-1} (@ 353 K), 4.26×10^{-1} (@ 363 K), 6.01×10^{-1} (@ 373 K)[30]
Pressure of supply gas at inlet of cell (absolute based) (MPa)	0.4[13]
Gas viscosity (H_2) [Pa·s]	9.96×10^{-6} (@ 353 K), 1.02×10^{-5} (@ 363 K), 1.03×10^{-5} (@ 373 K)[30]
Gas viscosity (O_2) [Pa·s]	2.35×10^{-5} (@ 353 K), 2.40×10^{-5} (@ 363 K), 2.45×10^{-5} (@ 373 K)[30]
Gas viscosity (H_2O) [Pa·s]	1.16×10^{-5} (@ 353 K), 1.19×10^{-5} (@ 363 K), 1.23×10^{-5} (@ 373 K)[30]
Binary diffusion constant (H_2-H_2O) [m^2/s]	9.27×10^{-5}[31]
Binary diffusion constant (O_2-H_2O) [m^2/s]	3.57×10^{-5}[31]
Porosity (catalyst layer) [-]	0.78[10,32,33]
Permeability (catalyst layer) [m^2]	8.69×10^{-12}[10,32,33]
Thermal conductivity (catalyst layer) [(W/(m·K))]	1.70[34]
Porosity (MPL) [-]	0.60[10,32,33]
Permeability (MPL) [m^2]	1.00×10^{-13}[10,32,33]
Thermal conductivity (MPL) [W/(m·K)]	1.00[35]
Porosity (GDL) [-]	0.78[10,32,33]
Permeability (GDL) [m^2]	8.69×10^{-12}[10,32,33]
Thermal conductivity (GDL) [W/(m·K)]	1.70[34]
Porosity (separator) [-]	0.15[36]
Permeability (separator) [m^2]	1.50×10^{-5}[36]
Thermal conductivity (separator) [W/(m·K)]	0.151[36]
Conductivity (PEM) [S/m]	10[37]
Conductivity (catalyst layer) [S/m]	53[38]
Conductivity (MPL) [S/m]	1000[39]
Conductivity (GDL) [S/m]	1250[35]
Conductivity (separator) [S/m]	83,000[36]
Reference equilibrium voltage (Anode) [V]	0
Reference equilibrium voltage (Cathode) [V]	1.229
Reference exchange current density (Anode) [A/m^2]	1000[34]
Reference exchange current density (Cathode) [A/m^2]	1[34]
Charge transfer constant (Anode) [-]	0.5[40]
Charge transfer constant (Cathode) [-]	0.5[41]

Table 3. Considered operation condition of power generation.

Operation parameters	Conditions	
The initial temperature of cell (T_{ini}) [K]	353, 363, 373	
Total cell voltage [V]	Experimental data are used[9,14]	
Supply gas condition	Anode	Cathode
Gas type	H_2	O_2
Temperature of supply gas at inlet of cell [K]	353, 363, 373	353, 363, 373
RH of supply gas [%RH]	40, 80	40, 80
Pressure of supply gas at inlet of cell (absolute based) [MPa]	0.4	0.4
Flow rate of supply gas at inlet of cell [NL/min] (Stoichiometric ratio [-])	0.210 (1.5)	0.105 (1.5)

Higher operation temperatures would cause PEM drying, which would also increase ionic resistance, ohmic loss, and material degradation[42]. As a result, it would be necessary to manage and control the temperature profile in the cell for the purpose of promoting power generation performance. Especially, an O_2 reduction reaction produces heat and H_2O as well as consumes O_2, resulting in complex phenomena occurring on the cathode side. These phenomena occur mainly at the interface between the PEM and catalyst layer on the cathode side. Since the power generation performance is influenced by temperature and humidification at the interface, this study focuses on the mass distribution, such as O_2 and H_2O distributions, the temperature distribution, and the current density distribution at the interface between the PEM and catalyst layer at the cathode side.

The analysis points from A to K, as shown in **Figure 3**, were assigned in this study, which was the same as that in the authors' previous studies[11,12] to examine the impact of separator thickness on the mass, such as O_2 and H_2O distributions, the temperature profile, and the current density profile. **Figure 3** shows the analysis points from A to K. We have conducted the analysis on the averaged value of the cross-sectional area at the interface between the PEM and catalyst layer at the cathode side, covering parts under the gas channel as well as those under the rib.

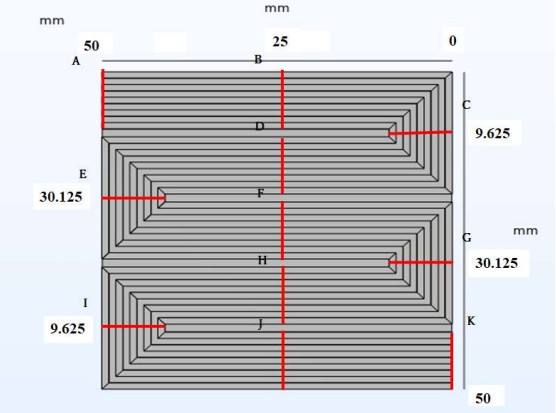

Figure 3. Analysis points from A to K for the quantitative evaluation along the gas flow through the gas channel.

3. Results and discussion

As to the validation of the model, the authors have used a similar and the same model in previous studies[12,43]. The results and discussions using the model have been recognized by the reviewers of these journals. In addition, the commercial software COMSOL applied in this study was used in many previous studies, and their results were well validated[14,15,18,27,28,44,45]. Therefore, the model was thought to be validated.

3.1. Comparison of temperature profile

Figures 4–6 show temperature distributions calculated by the 3D numerical simulation model at T_{ini} = 353 K, 363 K, and 373 K, respectively. In these figures, the saddle thickness and the channel height are expressed by Sa and Ch, respectively. The effect of separator thickness on the temperature profile is examined. Moreover, the RH of supply gases is also varied.

It can be seen from **Figures 4–6** that the increase in temperature on the interface between the PEM and catalyst layer at the cathode side from the inlet to the outlet of the cell is smaller with the increase in T_{ini} irrespective of the RH of the supply gas. It is known that the saturation pressure of H_2O increases with temperature exponentially[46], resulting in easy dehydration of PEM at higher temperatures than usual. Namely, it can be easy to reduce the proton conductivity of PEM at higher temperatures, causing a decrease in power generation performance at higher temperatures because of large ohmic losses. As a result, the generated heat decreases. Since we assume the excess amount of gas is greater than s.r. = 1.0 as the inlet gas flow rate, the

generated heat is accumulated along with the gas flow through the gas channel[47]. Therefore, the temperature on the interface between the PEM and catalyst layer at the cathode side rises from the inlet of the cell to the outlet of the cell.

Regarding the impact of separator thickness, the temperature change from the inlet to the outlet of the cell, i.e., the temperature fluctuation along the gas flow, at T_{ini} = 353 K and 363 K is larger when the separator thickness is 2.0 mm, consisting of the saddle thickness = 1.0 mm and the channel height = 1.0 mm. Because the heat capacity of the separator thickness of 2.0 mm was the biggest among the separators investigated in this study, the dehydration of the PEM and catalyst layer would be lower compared to the thinner separator thicknesses[12]. Consequently, it is thought that the power generation performance was improved with the increase in the separator thickness[12]. The reason why the temperature decreases at the positions of C, G, and K as the increase in the separator thickness and RH of supply gases occurs is discussed in the following sections.

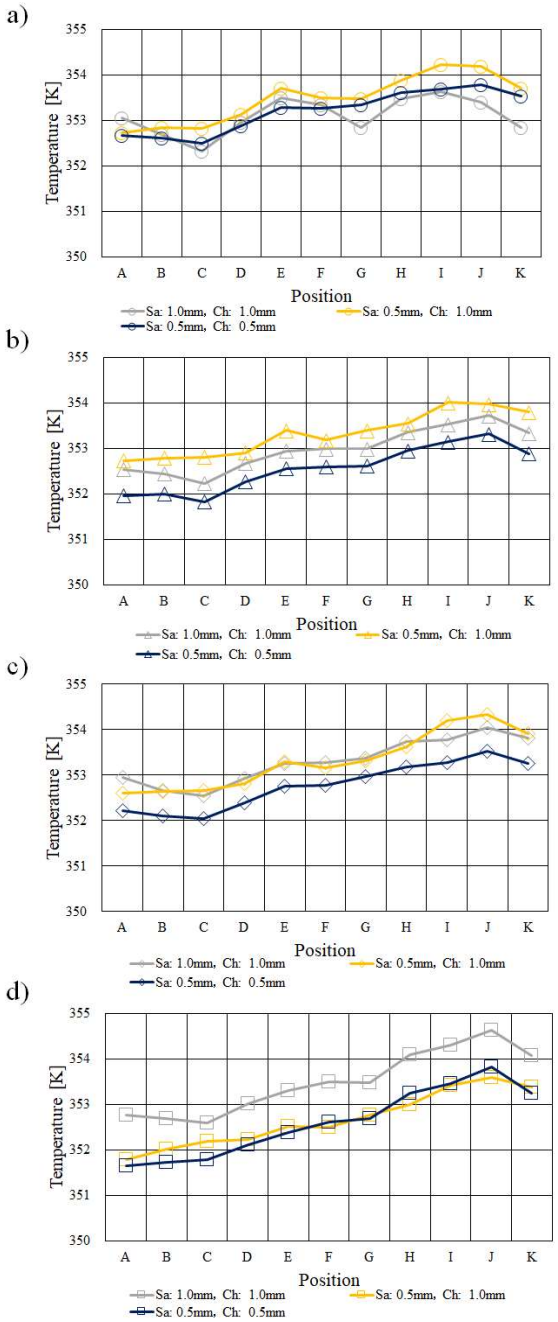

Figure 4. Comparison investigation on temperature profile among different separator thickness at T_{ini} = 353 K; **(a)** A80%RH-C80%RH; **(b)** A80%RH-C40%RH; **(c)** A40%RH-C80%RH; **(d)** A40%RH-C40%RH.

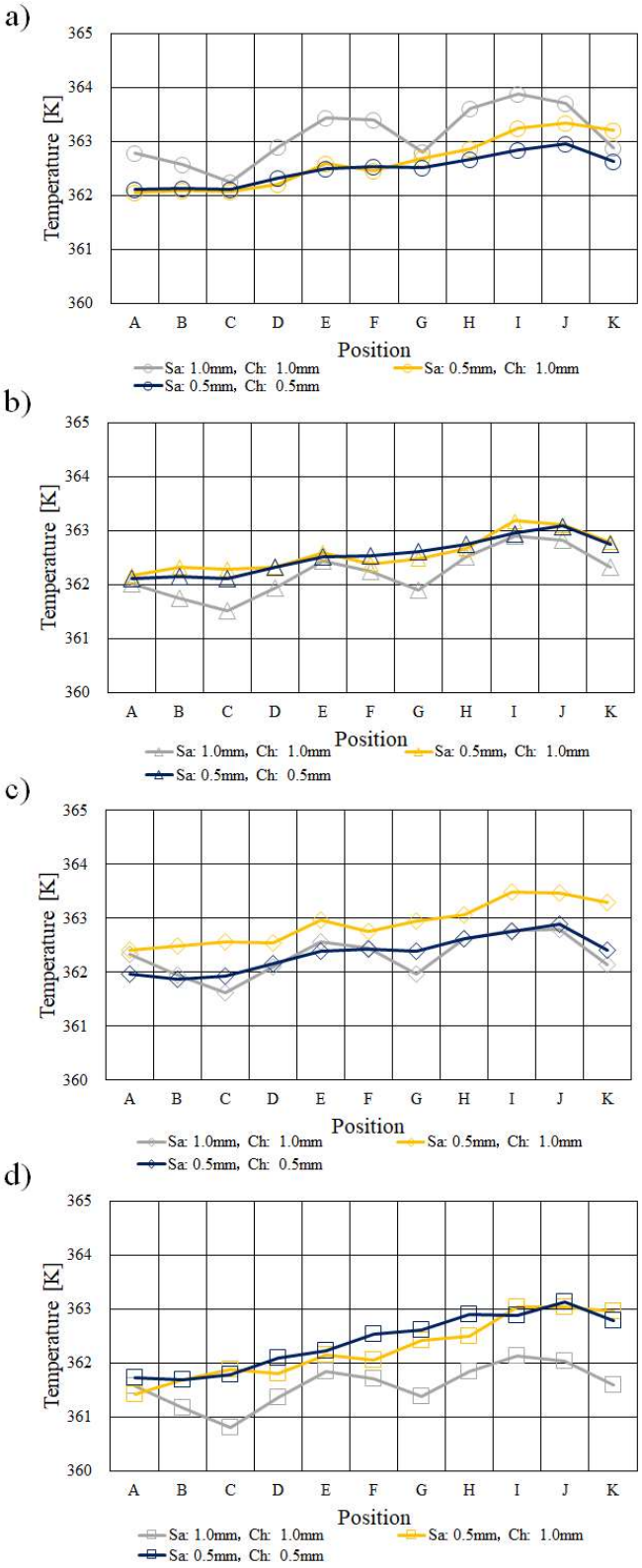

Figure 5. Comparison investigation on temperature profile among different separator thickness at T_{ini} = 363 K; **(a)** A80%RH-C80%RH; **(b)** A80%RH-C40%RH; **(c)** A40%RH-C80%RH; **(d)** A40%RH-C40%RH.

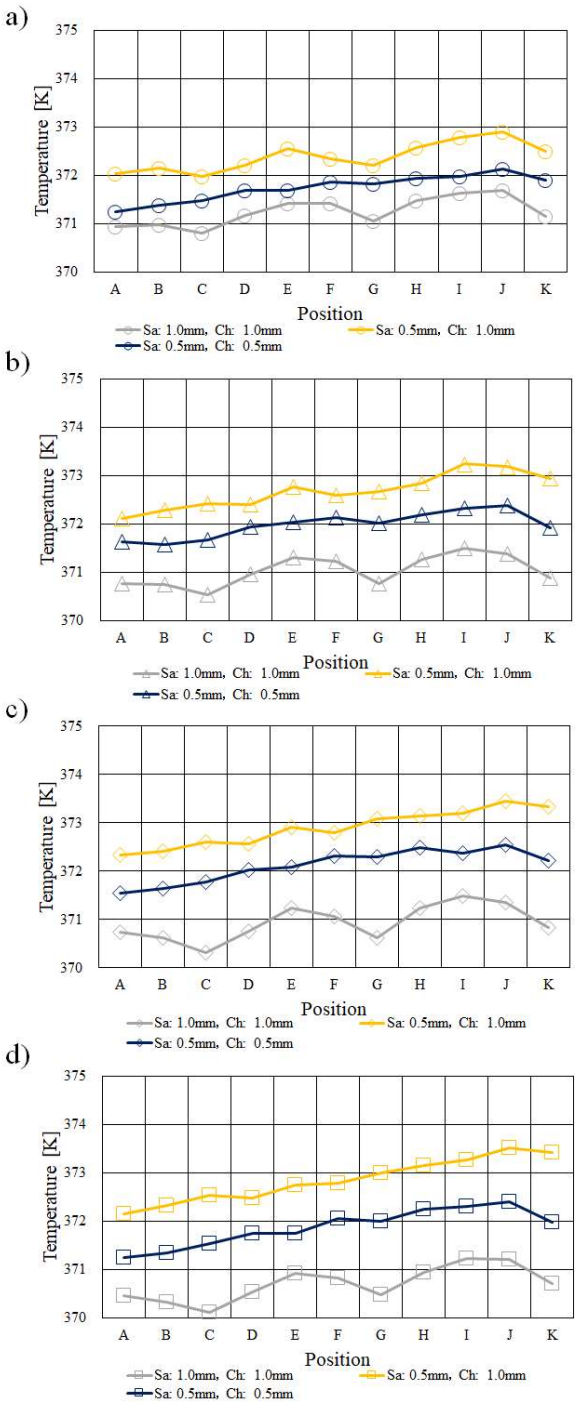

Figure 6. Comparison investigation on temperature profile among different separator thickness at T_{ini} = 373 K; **(a)** A80%RH-C80%RH; **(b)** A80%RH-C40%RH; **(c)** A40%RH-C80%RH; **(d)** A40%RH-C40%RH.

3.2. Comparison of O_2 distribution

Figures 7–9 show O_2 distributions calculated by the 3D numerical simulation model at T_{ini} = 353 K, 363 K, and 373 K, respectively.

It can be seen from **Figures 7–9** that the decrease in the molar concentration of O_2 (C_{O2}) from the inlet of the cell to the outlet of the cell, i.e., the consumption of O_2, becomes smaller with the increase in T_{ini} and the decrease in RH of supply gas, irrespective of separator thickness. The O_2 reduction reaction is carried out along the gas channel[43]. It is known that the saturation pressure of H_2O increases with temperature exponentially[43] as described above, resulting in easy dehydration of PEM at higher temperatures than usual. The proton conductivity of PEM reduces under higher temperatures and low RH conditions due to the dehydration of

PEM[43]. As a result, the ohmic overpotential becomes larger. On the other hand, the ionomer in the catalyst layer at the cathode side is not easily humidified by H_2O migrated through PEM from the anode side to the cathode side, which is a significant issue for the performance of the O_2 reduction reaction at the cathode side[12,43]. The big ohmic overpotential is provided due to ionic and electronic resistances. The ionic resistance is related to the resistance of PEM as well as the ionomer of the catalyst layer[48]. Therefore, the decrease in the molar concentration of O_2 from the inlet of the cell to the outlet of the cell is smaller with the increase in T_{ini} as well as the decrease in RH of the supply gas due to lower humidification.

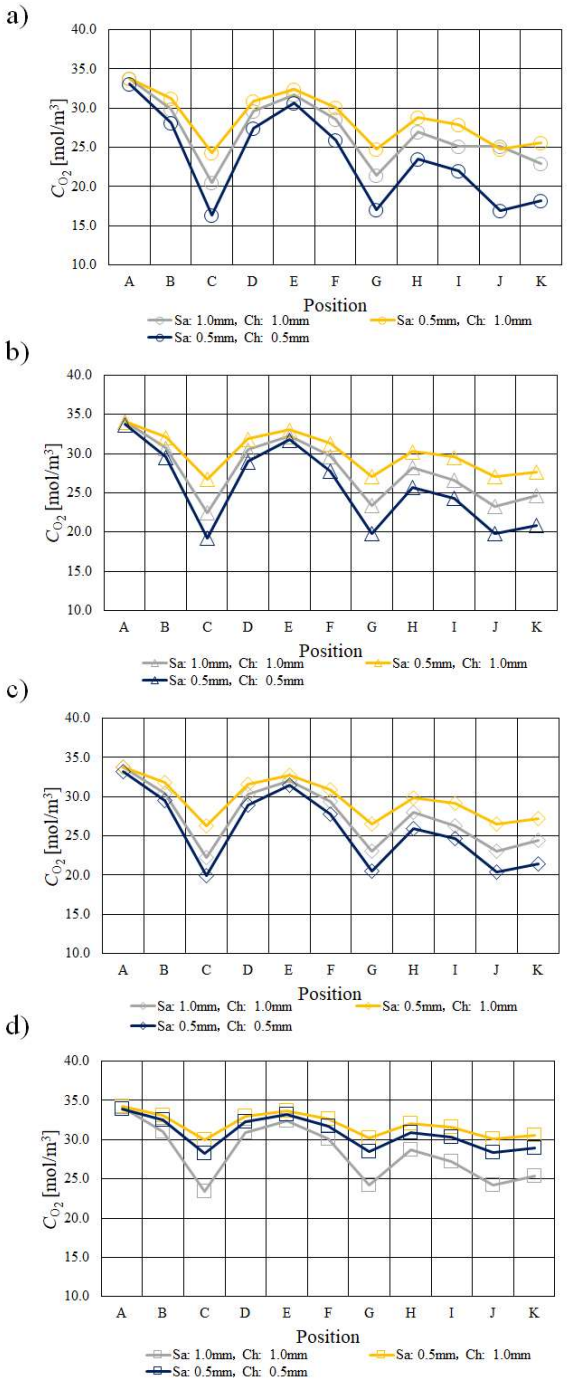

Figure 7. Comparison investigation on O_2 profile among different separator thickness at T_{ini} = 353 K; **(a)** A80%RH-C80%RH; **(b)** A80%RH-C40%RH; **(c)** A40%RH-C80%RH; **(d)** A40%RH-C40%RH.

As to the impact of separator thickness, the molar concentration of O_2 drops at analysis positions of C, G, and J (and K) when the separator thickness is 2.0 mm, especially at T_{ini} = 353 K and for A80%RH-C80%RH, which matches approximately the points of the temperature drop shown in **Figures 4–6**. The heat capacity of

the separator thickness of 2.0 mm is the biggest among the separators investigated in this study, resulting in the dry-up of the PEM and catalyst layer being lower compared to the thinner separator thicknesses[12]. In addition, the humidification of PEM and catalyst layer is higher for A80%RH-C80%RH. Consequently, the O_2 reduction reaction generating H_2O is improved with the increase in the separator thickness and RH of the supply gas. The analysis points C and G are located at the corner parts of the serpentine separator. Therefore, it can be thought that H_2O accumulates there[49,50]. Additionally, it is considered that H_2O remaining in gas flowing through the gas channel accumulates near the outlet of cell[9,51], which means the analysis points of J and K. As a result, the O_2 diffusion is inhibited at the analysis positions of C, G, and J (and K)[13], causing a reduction in the molar concentration of O_2. The impacts of separator thickness, as discussed above, become larger under higher temperatures and lower RH conditions, which are thought to be easy dehydration conditions.

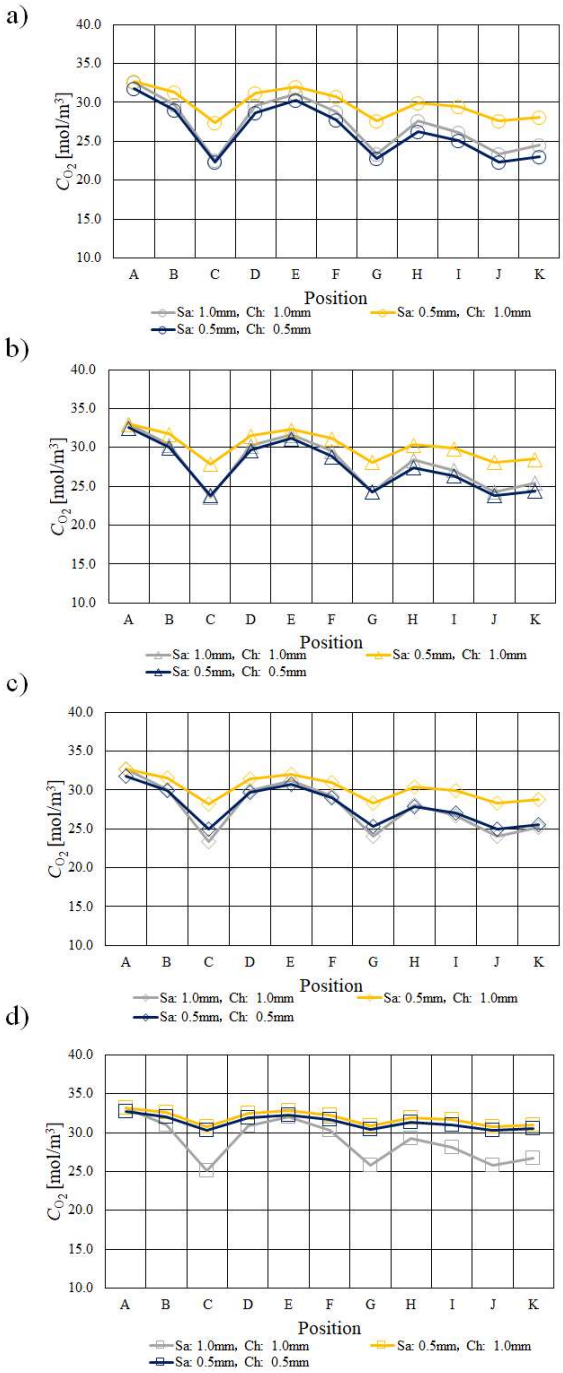

Figure 8. Comparison investigation on O_2 profile among different separator thickness at T_{ini} = 363 K; **(a)** A80%RH-C80%RH; **(b)** A80%RH-C40%RH; **(c)** A40%RH-C80%RH; **(d)** A40%RH-C40%RH.

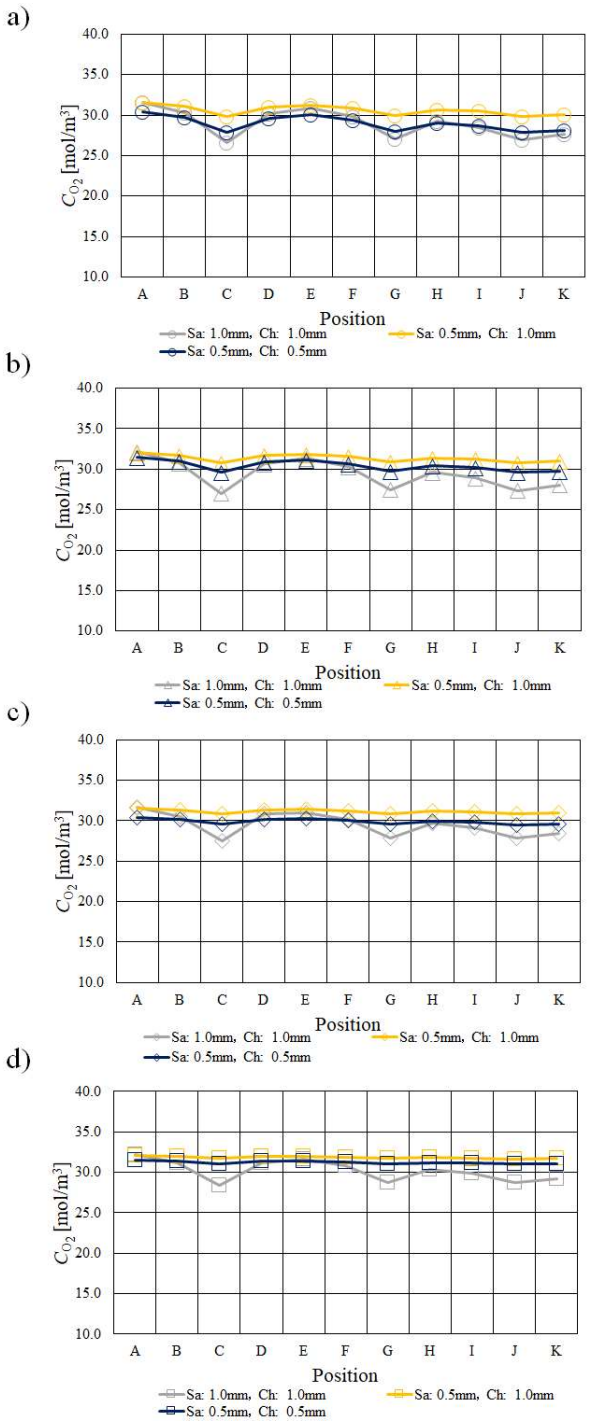

Figure 9. Comparison investigation on O_2 profile among different separator thickness at T_{ini} = 373 K; **(a)** A80%RH-C80%RH; **(b)** A80%RH-C40%RH; **(c)** A40%RH-C80%RH; **(d)** A40%RH-C40%RH.

3.3. Comparison of H_2O profile

Figures 10–12 show H_2O profiles calculated by the 3D numerical simulation model at T_{ini} = 353 K, 363 K, and 373 K, respectively.

It can be seen from **Figures 10–12** that the increase in the molar concentration of H_2O (C_{H2O}) from the inlet of the cell to the outlet of the cell becomes smaller with the increase in T_{ini} and the decrease in RH of the supply gas, irrespective of separator thickness. It is considered that H_2O remaining in gas flowing through the gas channel accumulates along the gas flow[49,50]. It is known that the saturation pressure of H_2O increases with temperature exponentially[46], resulting in easy dehydration of PEM at higher temperatures than usual. The proton conductivity of PEM reduces under higher temperatures and low RH conditions due to the dehydration

of PEM[14], causing a larger ohmic overpotential. On the other hand, the ionomer in the catalyst layer at the cathode side is not easy to be humidified by H_2O migrated through PEM from the anode side to the cathode side. It is significant for the performance of the O_2 reduction reaction at the cathode side[12,46]. The big ohmic overpotential is provided due to ionic and electronic resistances. The ionic resistance is related to the resistance of PEM as well as the ionomer of the catalyst layer[48]. Since the humidification is lower under higher temperatures and low RH conditions, the performance of the O_2 reduction reaction generating H_2O is smaller.

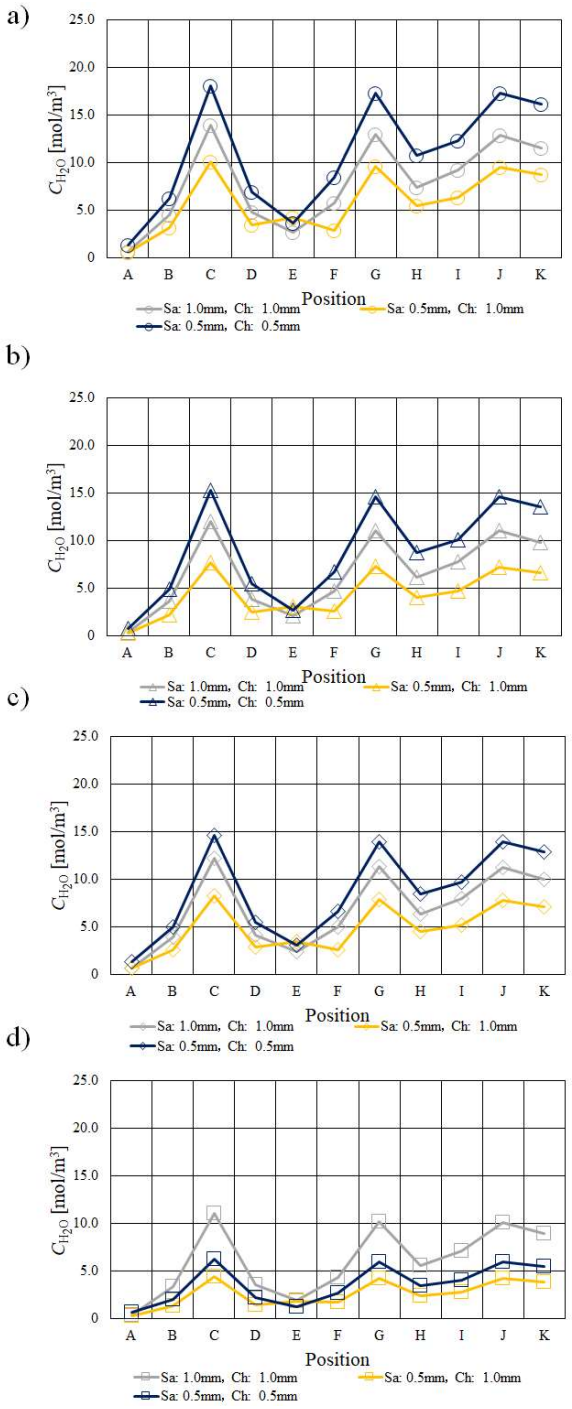

Figure 10. Comparison investigation on H_2O profile among different separator thickness at T_{ini} = 353 K; **(a)** A80%RH-C80%RH; **(b)** A80%RH-C40%RH; **(c)** A40%RH-C80%RH; **(d)** A40%RH-C40%RH.

As to the impact of separator thickness, it is known from **Figures 10–12** that the molar concentration of H_2O increases at analysis positions of C, G, and J when the separator thickness is 2.0 mm, especially at T_{ini} = 353 K and A80%RH-C80%RH, which matches approximately the points of the temperature drop shown in

Figures 4–6. The heat capacity of the separator thickness of 2.0 mm is the biggest among the separators investigated in this study, resulting in the dry-up of the PEM and catalyst layer being lower compared to the thinner separator thicknesses[12]. In addition, the humidification of the PEM and catalyst layer is larger for A80%RH-C80%RH. Consequently, the O_2 reduction reaction generating H_2O is improved with the increase in the separator thickness and RH of the supply gas. The analysis points of C and G are located at the corner parts of the serpentine separator. Therefore, it is thought that H_2O may accumulate there[49,50]. Additionally, we can claim that H_2O remaining in gas flowing through the gas channel accumulates near the outlet of cell[9,51], i.e., the analysis points of J and K. Consequently, the molar concentration of H_2O rises at the analysis points C, G, and J. As a result, the O_2 diffusion is inhibited, and the O_2 reduction reaction is not carried out well there. Consequently, the heat generated by the O_2 reduction reaction decreases at the analysis points of C, G, and J, causing the temperature to drop. The impacts of separator thickness, as discussed above, become larger under higher temperatures and lower RH conditions, which are thought to be easy dehydration conditions.

From this study, the saturation is below 1.0 under the investigated conditions, resulting in the assumption that the phase condition of H_2O is vapor. Therefore, the assumption that H_2O is a vapor is valid in this study.

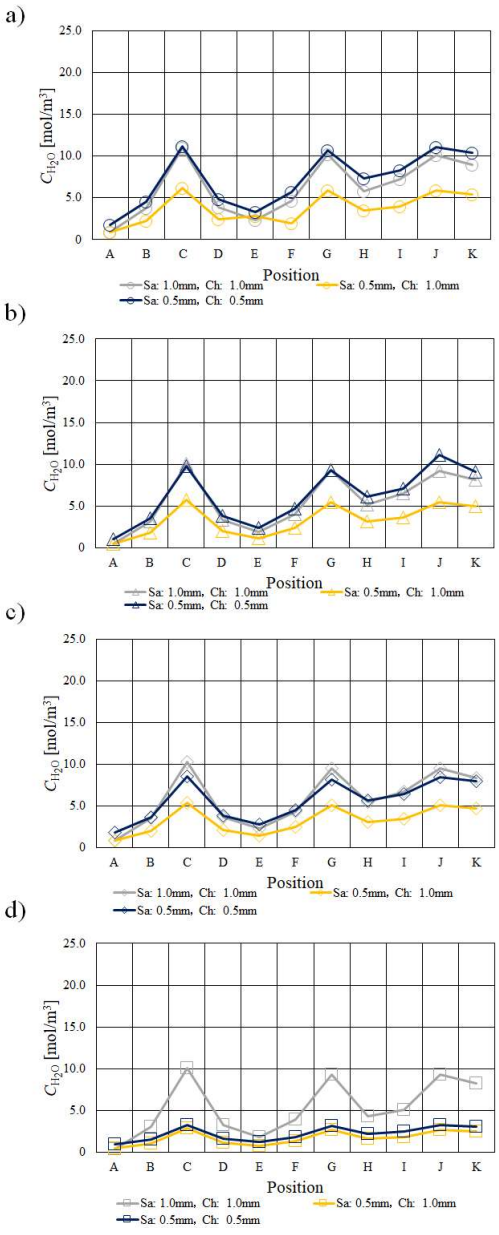

Figure 11. Comparison investigation on H_2O profile among different separator thickness at T_{ini} = 363 K; **(a)** A80%RH-C80%RH; **(b)** A80%RH-C40%RH; **(c)** A40%RH-C80%RH; **(d)** A40%RH-C40%RH.

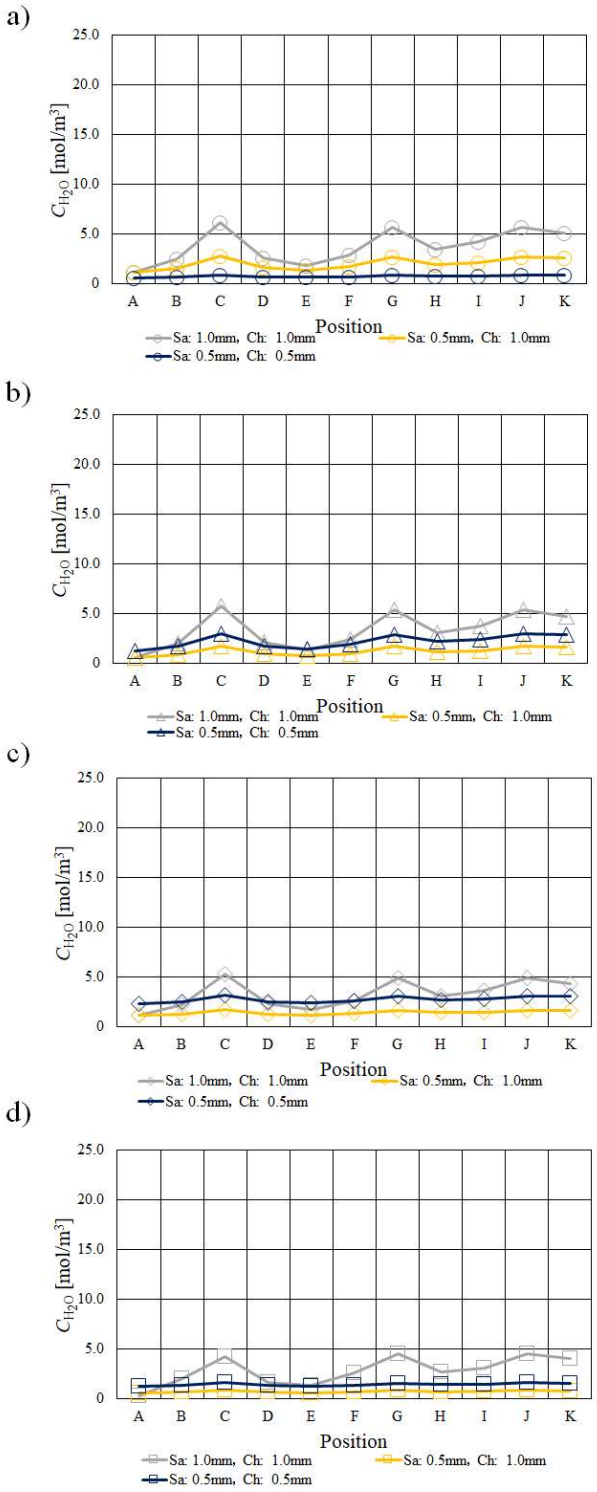

Figure 12. Comparison investigation on H_2O profile among different separator thickness at T_{ini} = 373 K; **(a)** A80%RH-C80%RH; **(b)** A80%RH-C40%RH; **(c)** A40%RH-C80%RH; **(d)** A40%RH-C40%RH.

3.4. Comparison of the current density profile

Figures 13–15 show current density profiles calculated using a 3D numerical simulation model at T_{ini} = 353 K, 363 K, and 373 K, respectively.

It can be found from **Figures 13–15** that the current density drops with the increase in T_{ini} and the decrease in RH of supply gas, irrespective of separator thickness. It is known that the saturation pressure of H_2O increases with temperature exponentially[46] as described above, resulting in easy dehydration of PEM at higher temperatures than usual. The proton conductivity of PEM reduces under higher temperatures and low RH

conditions since PEM is dehydrated[14]. Therefore, the ohmic over-potential becomes larger. On the other hand, the ionomer in the catalyst layer at the cathode side is not easy to be humidified by H_2O migrated through PEM from the anode side to the cathode side, which is significant for the performance of the O_2 reduction reaction at the cathode side[12,46]. The big ohmic overpotential is provided due to ionic and electronic resistances. The ionic resistance is related to the resistance of PEM as well as the ionomer of the catalyst layer[27]. Therefore, the current density reduces with the increase in T_{ini} and the decrease in RH of the supply gas due to lower humidification.

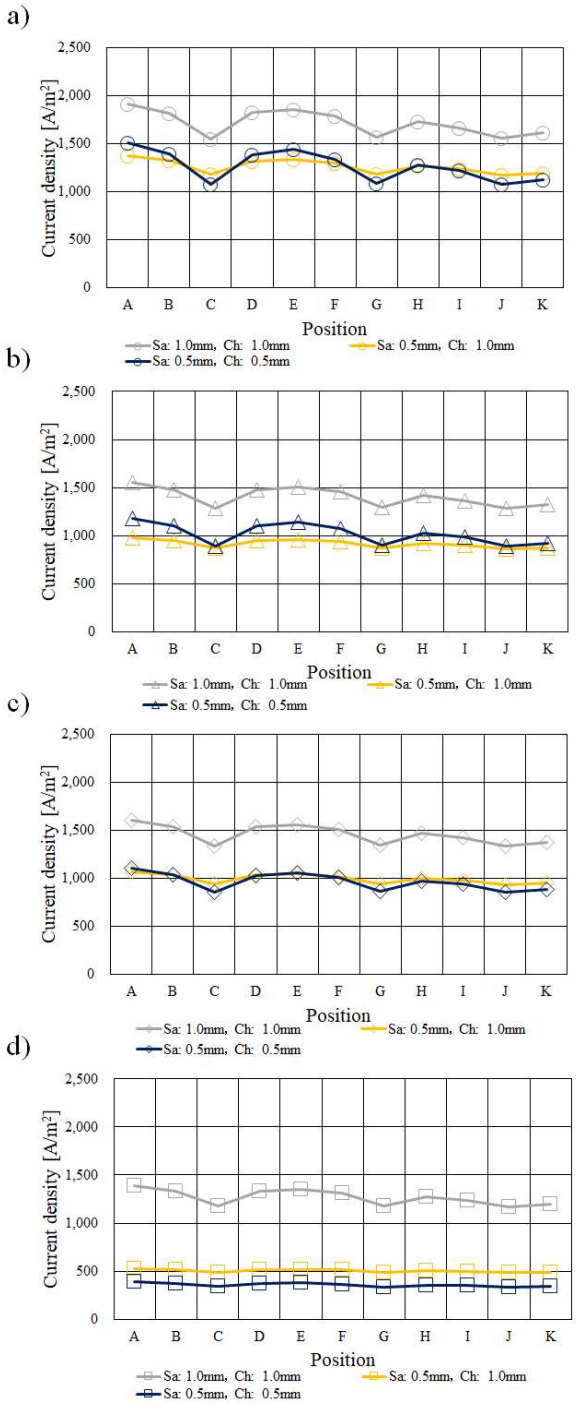

Figure 13. Comparison investigation on current density profile among different separator thickness at T_{ini} = 353 K; **(a)** A80%RH-C80%RH; **(b)** A80%RH-C40%RH; **(c)** A40%RH-C80%RH; **(d)** A40%RH-C40%RH.

According to **Figures 13–15**, the current density drops from the inlet of the cell to the outlet of the cell. H_2 and O_2 are consumed along with the gas channel, resulting in the driving force for the diffusion toward the

catalyst layer reducing along with the gas channel. As a result, the current density decreases from the inlet of the cell to the outlet of the cell.

Regarding the impact of separator thickness, it can be found from **Figures 13–15** that the current density drops at analysis positions of C, G, and J when the separator thickness is 2.0 mm, especially at T_{ini} = 353 K and for A80%RH-C80%RH, which matches approximately the points of the temperature drop shown in **Figures 4–6**. The heat capacity of the separator with a thickness of 2.0 mm is the biggest among the separators investigated in this study. Therefore, the humidification of the PEM and catalyst layer would be lower compared to the thinner separator thicknesses[12]. Additionally, the humidification of the PEM and catalyst layer is larger for A80%RH-C80%RH. Consequently, the O_2 reduction, which generates H_2O, is improved with the increase in the separator thickness and RH of the supply gas. The analysis points of C and G are located at the corner parts of the serpentine separator. Therefore, H_2O may accumulate there[49,50]. Moreover, it is considered that H_2O remaining in gas flowing through the gas channel accumulates near the outlet of cell[9,51], i.e., the analysis points of J and K, resulting in the increase in the molar concentration of H_2O at the analysis points of C, G, and J. As a result, the O_2 diffusion is inhibited, causing the O_2 reduction reaction to not be carried out well there. We can also claim that the concentration over-potential is larger there. Consequently, the current density drops at the analysis points of C, G, and J, causing the temperature drops shown in **Figures 4–6**. The impacts of separator thickness, as discussed above, become larger under higher temperatures and lower RH conditions, which are thought to be easy dehydration conditions.

In the current study, the optimum separator thickness is 2.0 mm to realize higher power generation performance among the investigated separator thicknesses. The separator with a thickness of 2.0 mm is the commercial and normal type, and the authors have customized the separator thicknesses of 1.5 mm and 1.0 mm to investigate the impact of channel height and saddle thickness on mass and heat transfer phenomena as well as power generation characteristics in this study. This study found that the separator thickness of 2.0 mm is the base case, and the other separator thicknesses are comparing cases. To decrease the thickness of the separator while keeping its strength, the separator thicknesses of 1.5 mm (saddle thickness = 0.5 mm, channel height = 1.0 mm) and 1.0 mm (saddle thickness = 0.5 mm, channel height = 0.5 mm) were selected in this study. If we select a separator thickness that is larger than 2.0 mm, it is expected that the power generation performance will be improved due to preventing the dry-up of PEM and catalyst. Since the heat capacity increases with the increase in separator thickness, the dehydration of PEM and catalyst due to temperature rise is prevented. As a result, it is expected that the performance of the O_2 reduction reaction will improve and the amount of H2O produced by the O_2 reduction reaction will increase. However, the optimum separator thickness for HT-PEMFC depends on the thermal design. The thinner thickness of the separator is better for improving the volumetric power density of the stack. If we develop a separator whose heat capacity is larger than the separator thickness of 2.0 mm, it is expected that the damage to PEM and catalyst due to heat up will be prevented, and the power generation performance could be improved due to preventing the dry-up of PEM and catalyst. For example, a porous metal separator may be a good candidate since a larger heat capacity can be obtained even if the thickness is smaller than 2.0 mm. This is the future work in this study. If a separator could be designed that could remove the generated heat smoothly, the separator thickness would be thinner. Since the weight ratio of the separator to that of the total cell is approximately 80%[21], a thinner separator is desirable.

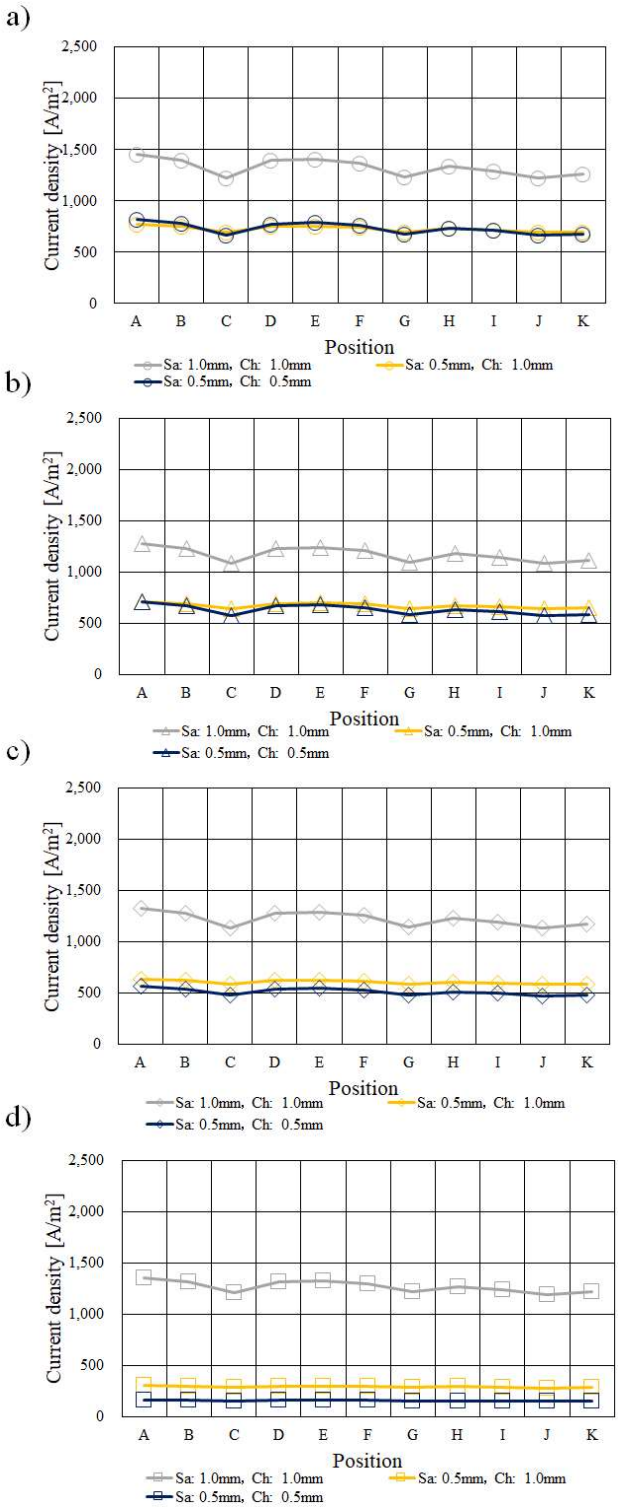

Figure 14. Comparison investigation on current density profile among different separator thickness at T_{ini} = 363 K; **(a)** A80%RH-C80%RH; **(b)** A80%RH-C40%RH; **(c)** A40%RH-C80%RH; **(d)** A40%RH-C40%RH.

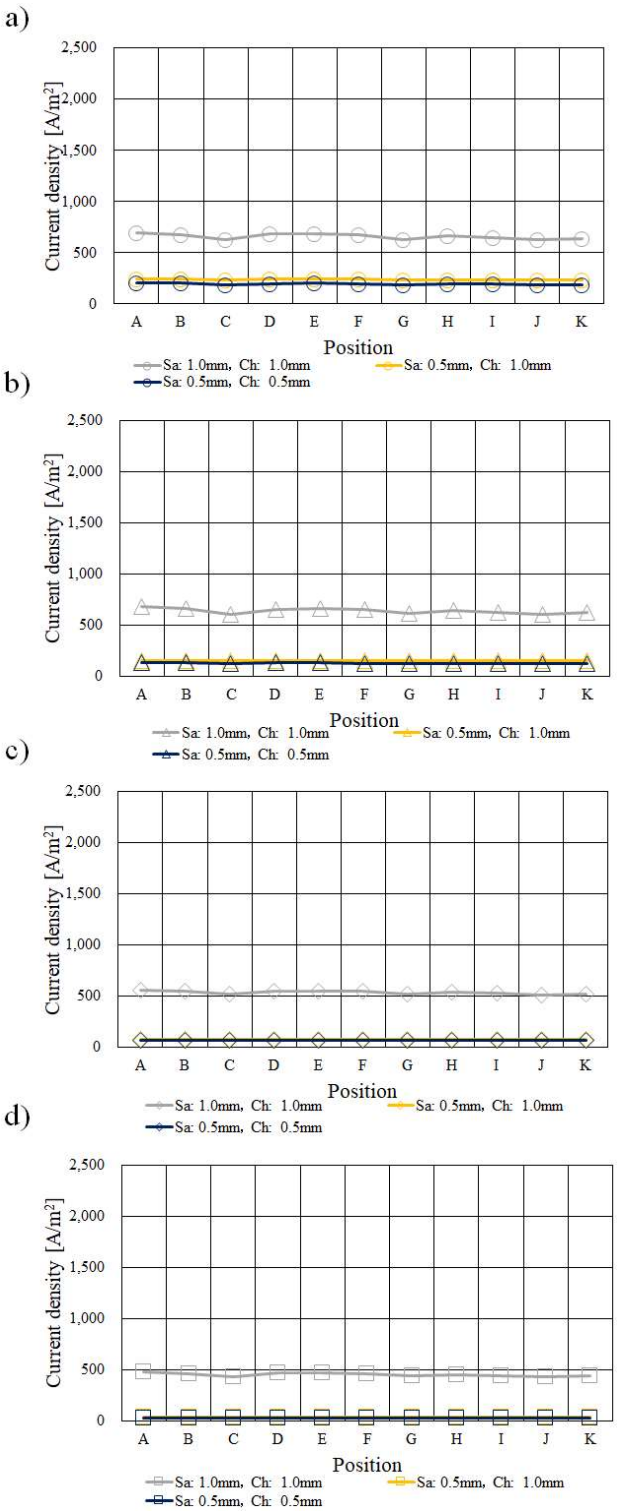

Figure 15. Comparison investigation on current density profile among different separator thickness at T_{ini} = 373 K; **(a)** A80%RH-C80%RH; **(b)** A80%RH-C40%RH; **(c)** A40%RH-C80%RH; **(d)** A40%RH-C40%RH.

4. Conclusion

The impact of separator thickness on the relationship between the temperature profile and not only the current density profile but also the profiles of gases, e.g., O_2 and H_2O, was examined in this study by numerical simulation using the CFD software COMSOL Multiphysics. In the study, the operation temperature was set at 353 K, 363 K, and 373 K, respectively, to compare the characteristics of HT-PEMFC with those of a general PEMFC. The following conclusions were drawn from the study:

1) The temperature change from the inlet of the cell to the outlet of the cell in the case of T_{ini} = 353 K

or 363 K was larger for the separator thickness of 2.0 mm compared to other separator thicknesses.

2) The decrease in the molar concentration of O_2 and the increase in the molar concentration of H_2O from the inlet to the outlet of the cell was smaller with the increase in T_{ini} and the decrease in RH of supply gas, respectively.
3) The current density decreased with the increase in T_{ini} and the decrease in RH of the supply gas, irrespective of separator thickness.
4) The optimum separator thickness was 2.0 mm to realize higher power generation performance among the investigated three separator thicknesses. If a separator that could remove the generated heat smoothly could be made, the separator thickness could be thinner.

Author contributions

Conceptualization and writing—original draft preparation, AN; methodology and software, DM; data curation, SI; methodology TK; writing—review and editing, EH. All authors have read and agreed to the published version of the manuscript.

Conflict of interest

The authors declare no conflict of interest.

References

1. New Energy and Industrial Technology Development Organization (NEDO). Available online: http://www.nedo.go.jp/cotent/100871973 (accessed on 16 August 2023).
2. Zhang G, Kandlikar SG. A critical review of cooling techniques in proton exchange membrane fuel cell stacks. *International Journal of Hydrogen Energy* 2012; 37(3): 2412–2429. doi: 10.1016/j.ijhydene.2011.11.010
3. Agbossou K, Kolhe M, Hamelin J, et al. Performance of a stand-alone renewable energy system based on energy storage as hydrogen. *IEEE Transactions on Energy Conversion* 2004; 19(3): 633–640. doi: 10.1109/tec.2004.827719
4. Zhang J, Zhang C, Hao D, et al. 3D non-isothermal dynamic simulation of high temperature proton exchange membrane fuel cell in the start-up process. *International Journal of Hydrogen Energy* 2021; 46(2): 2577–2593. doi: 10.1016/j.ijhydene.2020.10.116
5. Li Q, He R, Jensen JO, et al. Approaches and recent development of polymer electrolyte membranes for fuel cells operating above 100 °C. *Chemistry of Materials* 2003; 15(26): 4896–4915. doi: 10.1021/cm0310519
6. Lee CY, Weng FB, Kuo YW, et al. In-situ measurement of high-temperature proton exchange membrane fuel cell stack using flexible five-in-one micro-sensor. *Sensors* 2016; 16(10): 1731. doi: 10.3390/s16101731
7. Budak Y, Devrim Y. Micro-cogeneration application of a high-temperature PEM fuel cell stack operated with polybenzimidazole based membranes. *International Journal of Hydrogen Energy* 2020; 45(60): 35198–35207. doi: 10.1016/j.ijhydene.2019.11.173
8. Nanadegani FS, Lay EN, Sunden B. Computational anlysis of the impact of a micro porous layer (MPL) on the characteristics of a high temperature of PEMFC. *Electrochimica Acta* 2020; 333. doi: 10.1016/j.electacta.2019.133552
9. Nishimura A, Okado T, Kojima Y, et al. Impact of MPL on temperature distribution in single polymer electrolyte fuel cell with various thicknesses of polymer electrolyte membrane. *Energies* 2020; 13(10): 2499. doi: 10.3390/en13102499
10. Nishimura A, Yamamoto K, Okado T, et al. Impact analysis of MPL and PEM thickness on temperature distribution within PEFC operating at relatively higher temperature. *Energy* 2020; 205: 117875. doi: 10.1016/j.energy.2020.117875
11. Nishimura A, Toyoda K, Kojima Y, et al. Numerical simulation on impacts of thickness of nafion series membranes and relative humidity on PEMFC operated at 363 K and 373 K. *Energies* 2021; 14(24): 8256. doi: 10.3390/en14248256
12. Nishimura A, Mishima D, Toyoda K, et al. Numerical simulation on effect of separator thickness on

coupling phenomena in single cell of PEFC under higher temperature operation condition at 363 K and 373 K. *Energies* 2023; 16(2): 606. doi: 10.3390/en16020606
13. Nishimura A, Kojima Y, Ito S, et al. Impacts of separator thickness on temperature distribution and power generation characteristics of a single PEMFC operated at higher temperature of 363 and 373 K. *Energies* 2022; 15(4): 1558. doi: 10.3390/en15041558
14. Agarwal H, Thosar AU, Bhat SD, et al. Interdigitated flow field impact on mass transport and electrochemical reaction in high-temperature polymer electrolyte fuel cell. *Journal of Power Sources* 2022; 532: 231319. doi: 10.1016/j.jpowsour.2022.231319
15. Cai L, Zhang J, Zhang C, et al. Numerical investigation of enhanced mass transfer flow field on performance improvement of high-temperature proton exchange membrane fuel cell. *Fuel Cells* 2023; 23(3): 251–263. doi: 10.1002/fuce.202200131
16. Hazar H, Yilmaz M, Sevinc H. A comparative analysis of a novel flow field pattern with different channel size configurations. *Fuel* 2022; 319: 123867. doi: 10.1016/j.fuel.2022.123867
17. Zuo Q, Li Q, Chen W, et al. Optimization of blocked flow field performance of proton exchange membrane fuel cell with auxiliary channels. *International Journal of Hydrogen Energy* 2022; 47(94): 39943–39960. doi: 10.1016/j.ijhydene.2022.09.143
18. Yan F, Pei X, Yao J. Numerical simulation of performance improvement of PEMFC by four-serpentine wave flow field. *Ionics* 2022; 29(2): 695–709. doi: 10.1007/s11581-022-04849-0
19. Yu D, Yu S. Analysis of flow variation in a straight channel with baffled obstacles on a bipolar plate in a proton-exchange membrane fuel cell. *International Journal of Automotive Technology* 2023; 24(3): 759–771. doi: 10.1007/s12239-023-0063-0
20. Yu X, Luo X, Tu Z. Development of a compact high-power density air-cooled proton exchange membrane fuel cell stack with ultrathin steel bipolar plates. *Energy* 2023; 270: 126936. doi: 10.1016/j.energy.2023.126936
21. Tseng CJ, Heush YJ, Chiang CJ, et al. Application of metal foams to high temperature PEM fuel cells. *International Journal of Hydrogen Energy* 2016; 41(36): 16196–16204. doi: 10.1016/j.ijhydene.2016.06.149
22. Fly A, Meyer Q, Whiteley M, et al. X-ray tomography and modelling study on the mechanical behaviour and performance of metal foam flow-fields for polymer electrolyte fuel cells. *International Journal of Hydrogen Energy* 2019; 44(14): 7583–7595. doi: 10.1016/j.ijhydene.2019.01.206
23. Kahraman H, Orhan MF. Flow field bipolar plates in a proton exchange membrane fuel cell: Analysis & modeling. *Energy Conversion and Management* 2017; 133: 363–384. doi: 10.1016/j.enconman.2016.10.053
24. Han Y, Zhuge W, Peng J, et al. A novel heat pipe bipolar plate for proton exchange membrane fuel cells. *Energy Conversion and Management* 2023; 284: 116945. doi: 10.1016/j.enconman.2023.116945
25. Zhang J, Xie Z, Zhang J, et al. High temperature PEM fuel cells. *Journal of Power Sources* 2006; 160(2): 872–891. doi: 10.1016/j.jpowsour.2006.05.034
26. Kanchan BK, Randive P, Pati S. Implications of non-uniform porosity distribution in gas diffusion layer on the performance of a high temperature PEM fuel cell. *International Journal of Hydrogen Energy* 2021; 46(35): 18571–18588. doi: 10.1016/j.ijhydene.2021.03.010
27. Das SK, Gibson HA. Three dimensional multi-physics modeling and simulation for assessment of mass transport impact on the performance of a high temperature polymer electrolyte membrane fuel cell. *Journal of Power Sources* 2021; 499: 229844. doi: 10.1016/j.jpowsour.2021.229844
28. Panesi ARQ, Silva RP, Cunha EF, et al. Three-dimensional CFD modeling of H_2/O_2 HT-PEMFC based on H3PO4-doped PBI membranes. *Ionics* 2021; 27(8): 3461–3475. doi: 10.1007/s11581-021-04107-9
29. Penga Ž, Tolj I, Barbir F. Computational fluid dynamics study of PEM fuel cell performance for isothermal and non-uniform temperature boundary conditions. *International Journal of Hydrogen Energy* 2016; 41(39): 17585–17594. doi: 10.1016/j.ijhydene.2016.07.092
30. Cooper NJ, Santamaria AD, Becton MK, et al. Neutron radiography measurements of in-situ PEMFC liquid water saturation in 2D & 3D morphology gas diffusion layers. *International Journal of Hydrogen Energy* 2017; 42(25): 16269–16278. doi: 10.1016/j.ijhydene.2017.05.105
31. The Japan Society of Mechanical Engineers. *JSME Heat Transfer Handbook*, 1st ed. Maruzen; 1993. p. 387.
32. Freunberger SA, Reum M, Evertz J, et al. Measuring the current distribution in PEFCs with sub-millimeter resolution. *Journal of The Electrochemical Society* 2006; 153(11): A2158. doi: 10.1149/1.2345591

33. Xia L, Ni M, He Q, et al. Optimization of gas diffusion layer in high temperature PEMFC with the focuses on thickness and porosity. *Applied Energy* 2021; 300: 117357. doi: 10.1016/j.apenergy.2021.117357
34. TORAY. Available online: http://www.torayca.com/en/lineup/composites/com_009_01.html (accessed on 16 August 2023).
35. Kang K, Ju H. Numerical modeling and analysis of micro-porous layer effects in polymer electrolyte fuel cells. *Journal of Power Sources* 2009; 194(2): 763–773. doi: 10.1016/j.jpowsour.2009.05.046
36. Bit Tech. *Product Catalog*. Gosyogawara; 2008. p. 1.
37. Reid RC, Prausnitz JM, Poling BE. *The Properties of Gases and Liquids*, 1st ed. McGraw-Hill; 1987. p. 591.
38. Merck. Available online: http://www.sigmaaldrich.com/japan/materialscience/alternative/nafion.html (accessed on 16 August 2023).
39. Senn SM, Poulikakos D. Polymer electrolyte fuel cells with porous materials as fluid distributors and comparisons with traditional channeled systems. *Journal of Heat Transfer* 2004; 126(3): 410–418. doi: 10.1115/1.1738424
40. Takayama T. Numerical simulation of transient internal states of PEFC cell and stack considering control of anode system. *Research Report of Mizuho Research and Technologies* 2018; 9: 1–14.
41. Rostami L, Mohamad Gholy Nejad P, Vatani A. A numerical investigation of serpentine flow channel with different bend sizes in polymer electrolyte membrane fuel cells. *Energy* 2016; 97: 400–410. doi: 10.1016/j.energy.2015.10.132
42. Huang Y, Xiao X, Kang H, et al. Thermal management of polymer electrolyte membrane fuel cells: A critical review of heat transfer mechanisms, cooling approaches, and advanced cooling techniques analysis. *Energy Conversion and Management* 2022; 254: 115221. doi.: 10.1016/j.eneconman.2022.115221
43. Nishimura A, Toyoda K, Mishima D, et al. Numerical analysis on impact of thickness of PEM and GDL with and without MPL on coupling phenomena in PEFC operated at higher temperature such as 363 K and 373 K. *Energies* 2022; 15(16): 5936. doi: 10.3390/en15165936
44. Zhang S, Qu Z, Xu H, et al. A numerical study on the performance of PEMFC with wedge-shaped fins in the cathode channel. *International Journal of Hydrogen Energy* 2021; 46: 27700–2778.
45. Chen H, Guo H, Ye F, et al. Improving two-phase mass transportation under Non-Darcy flow effect in orientated-type flow channels of proton exchange membrane fuel cells. *International Journal of Hydrogen Energy* 2021; 46(41): 21600–21618. doi: 10.1016/j.ijhydene.2021.04.004
46. Xing L, Das PK, Song X, et al. Numerical analysis of the optimum membrane/ionomer water content of PEMFCs: The interaction of Nafion® ionomer content and cathode relative humidity. *Applied Energy* 2015; 138: 242–257. doi: 10.1016/j.apenergy.2014.10.011
47. Nishimura A, Toyoda K, Mishima D, et al. Numerical analysis on temperature distribution in a single cell of PEFC Operated at higher temperature by 1D heat transfer model and 3D multi-physics simulation model. *Energy and Power Engineering* 2023; 15(05): 205–227. doi: 10.4236/epe.2023.155010
48. Salomov UR, Chiavazzo E, Fasano M, et al. Pore- and macro-scale simulations of high temperature proton exchange fuel cells—HTPEMFC—and possible strategies for enhancing durability. *International Journal of Hydrogen Energy* 2017; 42(43): 26730–26743. doi: 10.1016/j.ijhydene.2017.09.011
49. Quan P, Lai MC. Numerical study of water management in the air flow channel of a PEM fuel cell cathode. *Journal of Power Sources* 2007; 164(1): 222–237. doi: 10.1016/j.jpowsour.2006.09.110
50. Jiao K, Park J, Li X. Experimental investigations on liquid water removal from the gas diffusion layer by reactant flow in a PEM fuel cell. *Applied Energy* 2010; 87(9): 2770–2777. doi: 10.1016/j.apenergy.2009.04.041
51. Zhang Y, He S, Jiang X, et al. 3D multi-phase simulation of metal bipolar plate proton exchange membrane fuel cell stack with cooling flow field. *Energy Conversion and Management* 2022; 273: 116419. doi: 10.1016/j.enconman.2022.116419